The Wetting Behavior of Polymer Droplets: Effects of Droplet Size and Chain Length

The Wetting Behavior of Polymer Droplets: Effects of Droplet Size and Chain Length

Apostolos E. A. S. Evangelopoulos,[†,¶] Anastassia N. Rissanou,[‡,*]

Emmanouil Glynos,[#] Ioannis A. Bitsanis,[#]

Spiros H. Anastasiadis[#,&] and Vasileios Koutsos[†,*]

[†] *School of Engineering, Institute for Materials and Processes, The University of Edinburgh, King's Buildings, Edinburgh EH9 3FB, United Kingdom*

[¶]*School of Mathematical and Physical Sciences, University of Reading, Reading RG6 6AX, United Kingdom.*

[‡] *Institute of Applied and Computational Mathematics (IACM), Foundation for Research and Technology Hellas (FORTH), GR-71110 Heraklion, Crete, Greece.*

[#] *Institute of Electronic Structure and Laser, Foundation for Research and Technology-Hellas, P.O. Box 1527, 711 10 Heraklion Crete, Greece.*

[&]*Department of Chemistry, University of Crete, P.O. Box 2208, 710 03 Heraklion Crete, Greece.*

E-mail: rissanou@iesl.forth.gr; vasileios.koutsos@ed.ac.uk

Phone: +30 2810 393746. Fax: +30 2810 393881[*]

Phone: +44 (0)131 650 8704. Fax: +44 (0)131 650 6554[*]

Supporting Information

[*] To whom correspondence should be addressed

Abstract

Monte Carlo computer simulations were utilized to probe the behavior of homopolymer droplets adsorbed at solid surfaces as a function of the number of chains making up the droplets and varying droplet sizes. The wetting behavior is quantified via the ratio of the perpendicular to the parallel component of the effective radii of gyration of the droplets and is analyzed further in terms of the adsorption behavior of the polymer chains and the monomers that constitute the droplets. This analysis is complemented by an account of the shape of the droplets in terms of the principal moments of the radius of gyration tensor. Single-chain droplets are found to lie flatter and wet the substrate more than chemically identical multi-chain droplets, which attain a more globular shape and wet the substrate less. The simulation findings are in good agreement with atomic force microscopy (AFM) experiments. The present investigation illustrates a marked dependence of wetting and adsorption on certain structural arrangements and propose this dependence as a technique through which polymer wetting may be tuned.

Introduction

The adsorption of polymers onto a surface and the wetting of a surface by polymers constitute a longstanding problem, which poses a number of challenges for a theoretical understanding,[1-2] particularly when the environment is a poor solvent[3] for the polymer. It also concerns a wide range of applications. For example, in surface coating and paint technology, the adsorption of polymers onto surfaces will determine the quality of spreading of the paint or coating in an effort to create a stable and easy-to-apply agent and to minimize the likelihood of blistering or peeling. In adhesives, the adsorption of the adhesive polymer on the solid determines the strength of adhesion.[4] Polymer-interface problems and thin polymer films is an area of extended studies both theoretical and experimental, where adsorption has been thoroughly studied.[5-16] Moreover, the wetting of carbon nanotubes or graphene by polymers is a critical process in judging the nano-compatibility between the two and the development of relevant nanocomposites.[17-20] Although there is a large number of studies on these topics, our focus here is mostly on the wetting process and the way that this is affected by the internal arrangement of chains within the homopolymer droplets. A plethora of simulation and experimental works have studied the adsorption of polymers onto surfaces; however, a systematic study that quantifies wetting in the nanoscale in terms of the internal arrangement of chains within the adsorbate is still missing.

Wetting of a surface by a polymer droplet and the underlying mechanism of adsorption of the polymer chains contained within the droplet differ essentially from those of low-molecular-mass substances. The differences are, on one hand, associated with the macromolecular size and, on the other, they additionally involve conformational aspects of the polymer chain, its structure and functionality and the degree of interpenetration of one chain with another at high enough concentrations. Taking further into account effects of the substrate and

environment, the problem of understanding and, ultimately, controlling the behavior of a polymer substance onto a surface becomes a complicated issue. Several techniques aiming at tuning polymer wetting and adsorption have been investigated, involving either adjusting properties of the polymer chains (e.g., molecular weight, structure, chemistry of chain end-groups) or of its environment (e.g., substrate, solvent, ambient conditions). Boyce, et al.[21] studied two-component polymer solution droplets using X-ray photoelectron spectroscopy and contact angle measurements. The wetting of dextran-coated glass was tuned by adjusting the molecular weight of each polymer component. Dee & Sauer[22] offered a theoretical analysis of the effects of molecular weight and temperature on the surface tension (which governs wetting) of polymer melts and compared theory with experiment. Koberstein and co-workers[23-24] showed that the sign of the molecular weight dependence of the surface tension of polymer melts can be altered depending on the surface energy difference between chain ends and middle segments. Wilson & Garoff[25] studied the effects of molecular weight and chain termination chemistry on the wetting of polymer liquids; for the specific polymers employed, tuning droplet wetting was more sensitive to the chain end-group chemistry than molecular weight. Qian, et al.[26] via experiment, and Glynos, et al.[27-28], via both experiment and simulation, showed that the wetting properties of star-polymer melt droplets could be dramatically altered and tailored in a controllable fashion by varying the functionality of the star-shaped polymers, i.e., the number of arms per molecule. Rissanou, et al.[13] studied the effect of the substrate on the adsorption of a polymer chain by exploring a range of attractive potentials, leading the polymer through a transition from a three-dimensional droplet to an almost two-dimensional platelet. With the present work, we contribute to the above discussion through a different approach, whereby the wetting of a homopolymer melt droplet is tuned via adjustment of its internal arrangement of chains, i.e., the number and length of polymer chains comprising the droplet. To the best of our knowledge, such a method has not

been previously proposed as a means of controlling wetting. However, there are a few simulation and experimental works that have witnessed such a structural effect indirectly, and we discuss these next.

Milchev, et al.[29] simulated chain aggregates on a substrate of variable attractive potential, under poor solvent conditions. Their results included density profiles of the cross section of adsorbed aggregates. From the density profiles, it was found that multi-chain droplets (aggregates) of different chain lengths yet of equal total monomer number exhibited similar adsorbed heights. They also showed[30] that these systems exhibited very similar contact angles for a wide range of adsorbed states, from complete dewetting to complete wetting, implying similar adsorbed heights. Heine, et al.[31] studied the spreading dynamics of both the precursor foot and the bulk of polymer droplets, using molecular dynamics (MD) simulations. While the focus was on the non-equilibrium dynamics, one could still extract important information regarding the equilibrium state, namely the similarity in the wetting state among large droplets (~*200000* monomers) consisting of different molecular weight chains. Dhondi, et al.[32] studied the capillary absorption of smaller (~*10000* monomers) polymer droplets into non-wettable capillaries. Their main finding, via both theory and simulation, was that for droplets of the same size (radius), the critical capillary radius (below which there was no absorption) increased with the length of the polymer chains that constituted the droplets and that the capillary dynamics were sensitive to polymer chain length. However, in characterizing the equilibrium properties of those droplets, it was observed that droplets of the same number of total monomers but made up of chains of different length shared similar dimensions. Subsequently, Dhondi, et al.[32] placed these droplets on a solid substrate; after equilibration, they measured adsorbed heights and extracted contact angles, which were roughly constant, independent of the length of the chains contained within the droplet. These investigations allow drawing a hypothesis that the adsorbed droplet dimensions are

independent of the length of the constituent chains when one compares droplets of equal total size.

As a separate case, one can refer to polymers grafted onto surfaces under various solvent conditions.[10, 33-37] Relevant to our study are polymers grafted onto surfaces in poor solvents. Especially motivated by a variety of applications, these systems have indeed received attention. Grafted polymers in poor solvents assume various morphological structures, including an inverted solvent micelle or hole in the polymer layer, a lamella-like micelle structure, and fused, spherical micelle structures. These structures can be obtained by either varying the grafting density or chain length. Pattanayek, et al.[33, 35] have studied such conformations via self-consistent field theory, Monte Carlo simulations as well as scaling theory. In an interesting review, Tagliazucchi and Szleifer[34] have also analyzed how curvature affects the morphology of polymers on nano-curved surfaces and determines the apparent equilibrium constant of surface-confined chemical reactions, such as acid–base chemistry.

The above works constitute a minority in the literature, which dealing with physical adsorption under poor solvent conditions. The majority of investigations pertain to adsorption under good or Θ solvents, as can be witnessed from review articles[38-42] and books.[43-46]

The picture of single and multi-chain adsorption in good/theta solvents is well established.[47-48] A chain forms a flat pancake at an adsorbing surface in order to balance the number of contacts with the surface as a result of the competing tendencies to lower potential energy and increase entropy. In the vicinity of an attractive surface, a chain will tend to maximize the number of contacts with the surface, while minimizing the entropic loss due to confinement in a region smaller than its unperturbed size. Even though each monomer may gain energy less than k_BT upon contact, the whole chain may gain energy much larger than k_BT because of

many contact points. However, when many chains exist in solution, the monomer concentration in the first layer (next to the surface) is determined by an energy balance between attraction to the surface and repulsion from the surrounding chains.

In poor solvents, on the other hand, chain spreading would be resisted by its natural tendency to minimize contact with the solvent. A non-trivial interplay between effective monomer-monomer and monomer-surface interaction would determine the chain conformation. In fact, this problem is so complicated that a single theory to account for the diversity of conformational behavior is extremely challenging.[3, 13, 49] With the present work we aim at contributing to that corner of the phase diagram, which concerns adsorption in poor solvent conditions and has been developed less. Even more, in the present work we compare single chains and multi-chain droplets of similar size in the context of wetting whereas, except from a very recent account[3] where a correspondence is made between adsorption and wetting of a single chain, single chains (as opposed to multichain droplets) have not been treated as droplets wetting a substrate in the literature. More specifically, in our analysis we systematically explore droplets of different sizes, as well as of different arrangement of chains (i.e., chemically identical droplets comprising a different number of polymer chains). In this way information on the adsorption procedure is revealed within the droplets, shedding light on the mechanics of the transition from a single to few to many chains making up droplets of equal size. On top of that, critical values for the chain length (N), which determines the adsorption-desorption threshold, are revealed as a function of the adsorption strength.

Finally, we make a connection with our previous study[50] on the wetting of polymer nanodroplets. In that work, we derived a thermodynamic model which related the height of an adsorbed polymer nanodroplet to material properties such as the polymer elastic modulus and interfacial tension. Atomic force microscopy (AFM) experiments on nanodroplets were in

support of the model and enabled it to be used as a predictive tool for the elastic modulus of a polymer droplet given its adsorbed height. These nanodroplets ranged in characteristic size from approximately *100nm to <5nm*. It was observed that, while *>5nm* droplets made up of several chains retained a cap shape on the substrate, single-chain droplets *<5nm* obtained a flat, pancake-like shape and could not be treated by the thermodynamic model. This difference in shape could only be witnessed between *>5nm* multi-chain and *<5nm* single-chain adsorbates, as single chains and multi-chain droplets overlapping in size were not at our disposal. Immediately, the question was raised whether this phenomenon is an implication of size, structure, or a combination of both. In the present work we follow up on that and provide an answer to this question by performing further experiments as well as via relevant computer simulations.

The rest of the paper is structured as follows: The Simulation Method section provides technical details of the Monte Carlo (MC) method employed and describes the characteristics of all simulated droplets. The experimental procedure is then outlined in the Experimental Method. The Results section is divided into four subsections: In the Exposition, the central finding of this work is showcased, i.e., the comparison of polymer melt droplets of equal total number of monomers yet unequal number of chains. A subsequent Wetting Analysis subsection quantifies the wetting state of the simulated droplets in terms of the *xy* and *z* components of the radius of gyration. The Adsorption Analysis subsection provides a detailed account of the interior of the droplets through analysis of the adsorption behavior of the chains contained within its droplet. Further analysis on droplet shape follows in the Shape Analysis subsection in terms of two structural parameters as a function of the radius of gyration tensor. Finally, the Experimental Observations subsection of the Results presents atomic force microscopy (AFM) measurements of the adsorption of linear polybutadiene

(PB) on mica in support of the simulation findings. General conclusions are drawn in the Concluding Remarks section.

Simulation Method

Single polymer chains and multi-chain droplets were simulated on a simple cubic lattice under poor solvent conditions next to an adsorbing surface located at $z = 0$, defining the horizontal. Monte Carlo (MC) simulations were performed in the canonical (*NVT*) statistical ensemble. The simulation code is an improved version of an established code, which has been used to study similar polymer chain systems floating in solvents[51] or near surfaces.[13] As the algorithm explores points in configuration space, the Metropolis scheme is used to make sure that this sequence converges to a Boltzmann distribution. In going from configuration i to configuration j, if the energy, E, of the system decreases (E_j-E_i<0), then the new configuration is accepted with probability 1, while if the energy of the system increases (E_j-E_i>0), the new configuration is accepted with probability equal to the Boltzmann factor, $p_{ij} = exp(-\beta(E_j-E_i))$, where β=1/ k_BT, k_B is Boltzmann's constant, and T is the temperature. This procedure satisfies the detailed balance criterion.

To sample different configurations, Local Monte Carlo (LMC) moves respecting lattice positions and chain connectivity were employed, comprising end rotation,[52] crankshaft rotation,[52] normal jump[52] and one-segment reptation[53] ("slithering snake"). The algorithm selects the type of move as well as the monomer on which the move will be attempted based on a random number generator, as follows: Firstly, a monomer is selected at random. Then a LMC move is selected at random and attempted on the monomer. If the move is not possible, another LMC move is selected at random. Failing all LMC moves, a new monomer is selected and the process is repeated. If a move is possible, the new configuration, resulting

from the proposed move, is assessed, based on the energy criterion explained previously, and a successful Monte Carlo step (MSC) is recorded upon acceptance of the new configuration. The next monomer can then be chosen and the process is repeated. The local nature of these moves, i.e. the fact that only a very small number of monomers are displaced at any one MCS, is imposed due to poor solvent conditions, which lead to compact chain configurations. Therefore, their limited efficiency meant that care had to be taken to allow enough time for equilibration. From the least dense systems comprising the most chains to the most dense systems of single chains, the acceptance ratio of MC moves ranged between 50% and 15%, respectively. Subsequently, for systems with smaller acceptance ratios, longer simulation times were utilized. Simulation times varied between 6×10^9 – 20×10^9 Monte Carlo steps (MCS) and configurations were sampled every 5000000 MCS.

The initial configurations are created by generating random sequences of monomers that observe connectivity and self-avoidance of the chain. These sequences are subsequently placed near the substrate and allowed to equilibrate by running the MC algorithm for sufficient times. These times vary, depending on the conditions of the simulation (i.e., solvent quality, surface affinity, etc). For each set of conditions, we have tried at least two topologically distinct random sequences and made sure that they lead to statistically equivalent conformations after equilibration under the same parameters. Even more, the randomness of the MC algorithm (i.e., different sequence of MC moves in each run) ensures further independence between equilibrated samples corresponding to the same parameters.

We employed a coarse grained model whereby each monomer was reduced to a point, constrained on the vertices of the cubic lattice with lattice constant α ($\alpha = 1$) and associated through an effective well potential ($u(r)/k_BT$) with other non-consecutive contact monomers

(exempt first neighbors) and the substrate ($u_w(z)/k_BT$) when it is at a distance of one lattice site apart (i.e., only segments at *z=1* experience this potential), as depicted in Eq. (1).

$$\frac{u(r)}{k_BT} = \begin{Bmatrix} -E, & r \le a \\ 0, & r > a \end{Bmatrix} \quad and \quad \frac{u_w(z)}{k_BT} = \begin{Bmatrix} -E_w, & z = 1 \\ 0, & z \ne 1 \end{Bmatrix} \qquad (1)$$

The monomer-monomer energy is denoted by -*E*, while the monomer-substrate energy by -E_w. Both energies are attractive so they attain negative values. In the present work, we explore $E = 0.45$ and $E_w = 0.3$ and *0.416*, in units of $\beta^{-1}=k_BT$, where k_B is Bolztmann constant and *T* the absolute temperature. Therefore, each site of the chain adjacent to another non-consecutive site contributes an amount -*E* to the internal energy of the system and each site of the chain adjacent to the substrate contributes an amount -E_w to the internal energy of the system. For a given chain, *E* implicitly determines the solvent quality, with increasing absolute values corresponding to decreasing solvent quality, $E = 0$ being the athermal solvent.[51]

In our previous work,[13] we had identified the characteristic values of the energetic parameters: the adsorption-desorption threshold, which is a function of the solvent quality, is around $E_w^c = 0.25$ for *E=0.45*. Therefore, in the present simulations, where $E_w=0.3$ and $E_w=0.416$, the system is above the adsorption-desorption threshold, with a tendency for adsorption. The two cases of $E_w=0.3$ and $E_w=0.416$ are referred to as weak adsorption and strong adsorption, respectively, only in a relative sense, whereas no other interpretation should be attributed to the terms 'weak' and 'strong'. The *effective* Θ-solvent conditions, which are a function of the adsorption energy E_w, are realized around $E\Theta = 0.28$ and $E\Theta = 0.37$ for $E_w=0.3$ and $E_w=0.416$, respectively.[13] Thus, in the present simulations, where *E=0.45*, the chains are in the poor solvent regime.[13, 51] The excluded volume effect was

implemented through self-avoidance of the chains, which are otherwise freely jointed, i.e., with no associated potential of bending.

Simulations were performed inside a box of dimensions $L \times L \times L_Z$ with periodic boundary conditions (PBC) imposed on the x and y directions and homogeneous and impenetrable floor and ceiling (z- direction). We chose $L, L_Z > 8 \sim 10R_g$, where R_g is the radius of gyration[48] of the droplet, in order to avoid self-correlation effects and bridge formation.

Droplets of three different sizes were simulated, namely of a total number of $N_T = 1000$, $N_T = 5000$, and $N_T = 10000$ monomers. Each system comprised a variable number of chains, n, of equal length / number of monomers, N. The number of chains in a droplet ranged from n=1 to as many as possible (different for each N) on the condition that the droplet maintained cohesion and its chains did not dissociate. It is noted here that for short enough chains it was entropically favourable to break apart from the original cluster. The set $[N_T, N, E_w]$ (or, equivalently, $[N_T, n, E_w]$) uniquely specifies a droplet in our simulations (where E is constant). All $[N_T, N, E_w]$ combinations are shown in Table 1. As mentioned previously, there was a limit in the number of chains, n, that could constitute a droplet, beyond which the latter suffered segregation of one or more of its chains. This limit in cohesion was influenced by several factors, including the solvent quality (E), the substrate quality (E_w) and topological aspects such as entanglement between chains, highly dependent on their length, N. In simulation time, following an event of segregation, constituents of what formerly was a coherent droplet might or might not have recombined. Those systems, for which a segregated state was statistically favoured are denoted by ‘s’ in Table 1, and are not treated further in this work. Even more, chain lengths that do not correspond to an integer number of chains in a multi-chain droplet are denoted by ‘n/a’ and are also not treated. All results reported in this work are averages of an ensemble of approximately *1000* to *2000* microstates, depending on the relaxation time of each system, far enough apart in simulation time that statistical

correlations have sufficiently decayed. Error bars in graphs measure one standard deviation. Units are in lengths of a lattice unit cell or, equivalently, 'monomer' lengths.

Table 1: The entirety of simulated droplets. Each [N_T, N, E_w] combination uniquely specifies a droplet and the statistical ensemble to which that corresponds. ■ $E_w = 0.3$; ● $E_w = 0.416$. Systems for which a segregated state was statistically favoured are denoted by 's'. Chain lengths that were not permissible by division to give an integer number of chains in a droplet are denoted by 'n/a'.

N_T \ N	100	125	200	250	400	500	650	1000	1250	2000	2500	5000	10000
1000	ss	■ s	■ s	■ ●	n/a	■ ●	n/a	■ ●	n/a	n/a	n/a	n/a	n/a
5000	ss	■ s	■ ●	■ ●	n/a	■ ●	n/a	■ ●	■ ●	n/a	■ ●	■ ●	n/a
10000	■ s	■ s	■ ●	■ ●	■ ●	■ ●	■ ●	■ ●	■ ●	■ ●	■ ●	■ ●	■ ●

Furthermore, the autocorrelation functions of selected vectors along the polymer chains have been calculated and used as an indication of equilibration of the simulated systems. Figure 1s of the Supporting Information shows the autocorrelation function of the second Legendre polynomial $P_2(t) = \frac{3}{2}\left\langle \cos^2 \theta(t) \right\rangle - \frac{1}{2}$ for various vectors connecting monomers i and j along the longest (N=*10000*) polymer chain. In this expression, $\theta(t)$ is the angle of the vector under consideration at time t relative to its position at t=*0*. This was illustrated for the system with $N = N_T$ =*10000* and E_w=*0.416* because it is the most demanding from the point of view of equilibration. From Figure 1s it is obvious that collected configurations are distant enough such that all autocorrelation functions attain values ≤0.2 even after ~*5.000.000* MCS. All vectors have been decorrelated beyond the first ~*50* configurations (i.e., *250.000.000* MCS); this ensures that the statistical correlations have decayed. Moreover, a representative snapshot

of the $N=N_T=10000$, $E_w = 0.416$ system is provided in Figure 2s in Supporting Information. There is an evident change in the shape of the chain as well as in the position of the chain ends in agreement with the decorrelation of the vectors discussed above.

Experimental Method

Linear polybutadiene (PB) polymer chains of two different molecular weights, *78.8* and *962 kg/mol*, were utilized dissolved in an appropriate volume of toluene in order for the solutions to maintain concentrations well below the critical overlap concentration, c^* ($c/c^* \simeq 0.3$). The critical overlap concentration (c^*) was calculated using the polymer chain properties: $c^* = M_n/(V_p N_A)$, where, M_n is the molecular weight, V_p is the pervaded volume, and N_A the Avogadro's number.[48] Toluene was used as received (Fisher Scientific, Loughborough, U.K.). As per standard practice for such PB solutions, a small amount (~0.1%) of antioxidant (2,6-di-tert-butyl-p-cresol) was added to the solution to protect PB from oxidation.[54] In a typical experiment, a freshly cleaved mica surface (Agar Scientific, Essex, U.K.) was incubated in a polymer solution for times between ~*10* minutes up to ~*2* hours, depending on the sample. The mica surface was removed from the solution and placed in a *100 mL* toluene bath for *24 h* and then rinsed exhaustively with *100 mL* of toluene to ensure the removal of non-adsorbed PB chains. Subsequently, the samples were dried gently with a stream of nitrogen. The resulting polymer structures were investigated by atomic force microscopy. The PicoSPM (Agilent Technologies) was operated in tapping mode in air. Commercially available Si_3N_4 (MikroMasch, Talinn, Estonia) rectangular cantilevers, with a spring constant of *1.75 N/m* and resonance frequency of *130−160 kHz*, were used. The cantilevers were oscillated *5%* below their natural resonant frequency and during imaging moved in a raster fashion. Each sample was imaged at several different areas.

In AFM measurements, convolution due to the finite size of the cantilever tip is unavoidable. The tip convolution effect[55] increases the apparent width of features (such as polymer aggregates and single chain globules in the form of nanodroplets) and affects measurements such as volume and number of chains per aggregate. For this reason, deconvolution is applied in order to get accurate estimates of the real volume and number of chains within the polymer aggregates imaged by AFM. On a mica surface, the polymers form spherical cap shaped aggregates from which a real volume $V_r = V_a - \pi h^2 R_t$ can be determined using a simple method developed by Glynos, et al.,[56] where V_a is the apparent volume of the aggregate, h is the height of the aggregate, which is unaffected by convolution, and R_t is the radius of the AFM tip (around *50 nm* in our case). The volume of a single chain $V_c = M_n/(\rho N_A)$ can be found by its number-average molecular weight, M_n, and its density, ρ, where N_A is Avogadro's number. The density of PB is dry conditions is assumed to be the bulk density, $\rho = 0.89\ g/cm^3$.[56-57] The number of chains per aggregate can be calculated by dividing the real volume, V_r, by the volume of a single polymer chain, V_c. If the real volume of a nanodroplet is approximately equal to the volume of a single chain, we deduce that this is a single chain globule.

The size of the polymeric islands was determined by using the grain analysis of the software Scanning Probe Image Processor (SPIP, Image Metrology, Hørsholm, Denmark). It is well-known that the AFM tip can make an object lying on a surface look wider due to convolution of the geometry of the tip and the shape of the object being imaged. As in previous work,[56, 58] we have used geometrical arguments to deconvolute the real volume of the object imaged from its apparent volume, which contains the effects of the probe tip geometry. We repeatedly imaged the samples at room temperature over the course of weeks and did not observe significant changes in the adsorbed state; it was, therefore, considered that they had reached a steady state.

Results and Discussion

Exposition: single chain vs multi-chain droplets.

Figure 1 shows a comparison of polymer melt droplets of equal total number of monomers yet unequal number of chains. The simulation snapshot reveals the wetting state of a droplet consisting of one (*1*) chain of *N=10000* monomers compared to that of a droplet consisting of one hundred (*100*) chains of *N=100* monomers. The total number of monomers is the same (*1×10000=100×100*), as is their chemical identity, and the volume of the droplets. However, their shape is different. The single chain attains a flatter, pancake-like shape, while the multi-chain droplet attains a more globular shape.

In the following, the computer experiments of the systems of Table 1 are analyzed in order to understand how such differences in internal arrangement of chains affect wetting, adsorption and the shape of polymer melt droplets. We analyze the wetting behavior of droplets, in terms of the ratio of the perpendicular to the parallel component of the radius of gyration, the adsorption behavior, in terms of the adsorption of the constituent chains and monomers as well as the shape of droplets, in terms of the principal moments of the gyration tensor. Ultimately, we compare this analysis to experimental data.

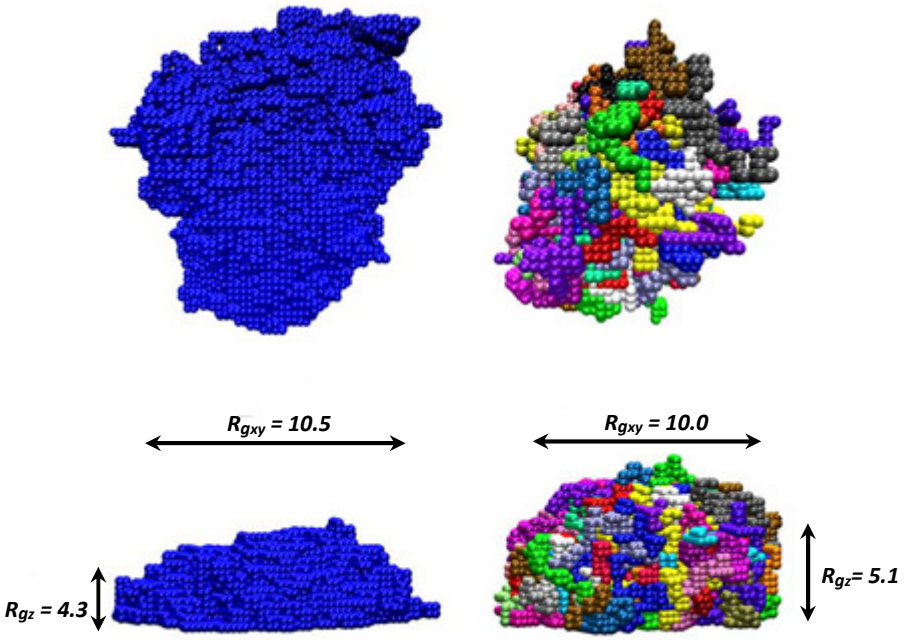

Figure 1: Top (top row) and side (bottom row) view of a droplet consisting of *1* chain of *N=10000* monomers (left) and a droplet consisting of *100* chains of *N=100* monomers (right) residing on a weakly attractive substrate, E_w=*0.3*, in poor solvent conditions, *E=0.45*. Horizontal, Rg_{xy}, and vertical, Rg_z, components of the radii of gyration of the combined system of chains at equilibrium wetting conditions.

Wetting analysis

The *N=100* and the *N=10000* single chain droplet of Figure 1 are examples of the two ends of a series of simulated droplets containing a constant total number of monomers, N_T = *10000*, and varying number of chains, *n = 1, 2, 4, …, 80, 100*, corresponding to respective chain lengths *N = 10000, 5000, 2500, …, 125, 100* (see Table 1 for a complete list). Figure 2c shows the ratio of the perpendicular to the parallel component of the radius of gyration, Rg_z/Rg_{xy}, of the combined system of chains for this series of droplets with N_T=*10000*, which

can be used to quantify the shape of the adsorbed polymer droplet and, therefore, describe its wetting state or contact angle.

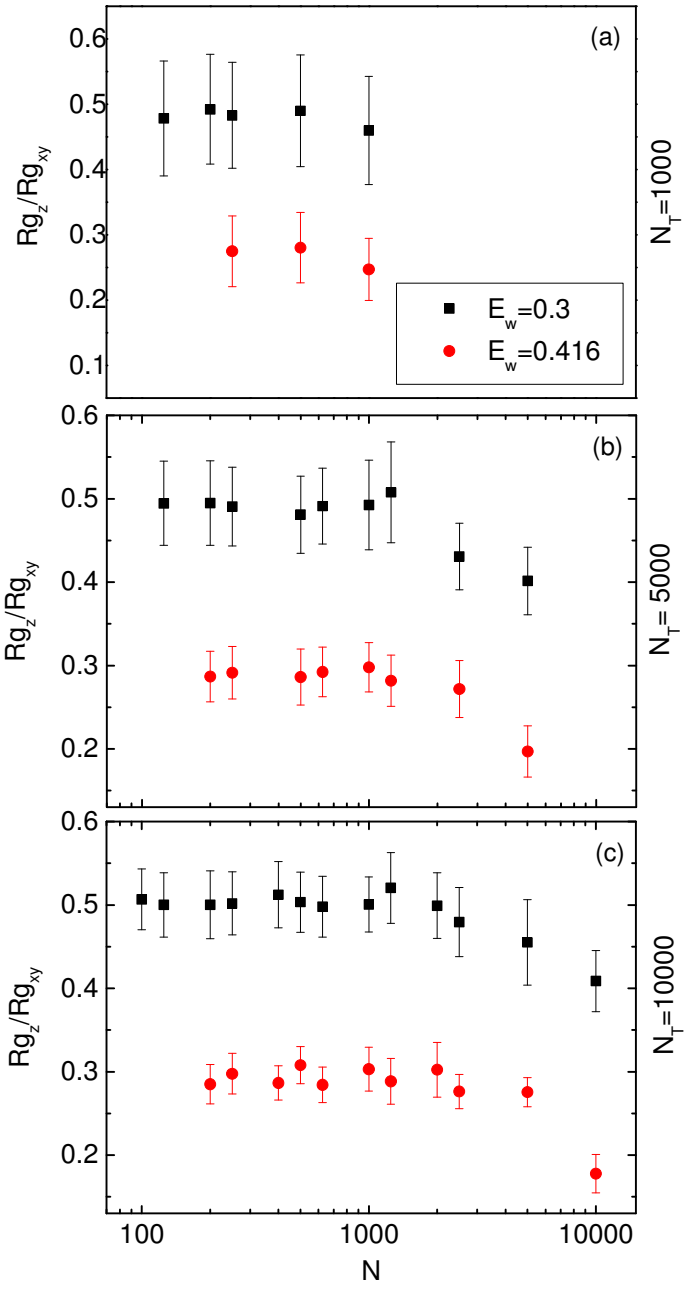

Figure 2: Ratio of the perpendicular to parallel component of the radius of gyration, Rg_z/Rg_{xy}, of droplets as a function of the molecular weight, N, of the constituent chains, for three series of simulated droplets, each of constant total number of monomers, $N_T=1000$ (a),

N_T=*5000* (b), and N_T=*10000* (c), under weak, E_w=*0.3* (black squares), and strong, E_w=*0.416* (red circles), adsorption in poor solvent conditions, *E=0.45*.

A lower ratio denotes increased wetting (i.e., smaller thickness), whereas a higher ratio denotes decreased wetting (i.e., larger thickness). Weaker, E_w=*0.3*, and stronger, E_w=*0.416*, adsorbing substrates are shown. As reasonably expected, droplets exhibit a higher Rg_z/Rg_{xy}, or decreased wetting, on the weaker adsorbing substrate, E_w=*0.3*, and a lower Rg_z/Rg_{xy}, or increased wetting, on the stronger adsorbing one, E_w=*0.416*. The same behavior is seen in Figures 2a and 2b, which are discussed in the following. Figure 2c quantifies a central result, a special case of which was previously depicted in Figure 1. The droplet comprising the single chain, *N=10000*, lies flatter and wets the substrate more than the multi-chain droplet that attains a more globular shape and wets the substrate less. Furthermore, most multi-chain droplets share a common Rg_z/Rg_{xy} value. Trends are similar for both substrate types, E_w=*0.3* and E_w=*0.416*, whereas the difference between the single chain and the multi-chain droplets is more pronounced in the latter case. Moreover, the droplet containing two-chains with *N=5000* on the E_w=*0.3* substrate seems to lie in an intermediate wetting state. Figure 2c makes clear that the phenomenon pictorially illustrated in Figure 1 is not exclusively a chain length effect (*N*) but a combined effect of *N* and *n* (number of chains included in the droplet). A range of *N* values from *100* to *2500* and *n≥3* exhibit an approximately constant degree of wetting. Simulations were performed for two more series of droplets of total monomer number N_T=*5000* (Figure 2b) and N_T=*1000* (Figure 2a). The N_T=*5000* series exhibits similar behavior to the N_T=*10000* case and the above discussion holds. The N_T=*1000* series differs in that the contrast between single- and multi-chain droplets is not as sharp, because of the higher Rg_z/Rg_{xy} ratio for the single chains (to be discussed at the end of this subsection, under single chains). Note here that the ratio Rg_z/Rg_{xy} for all systems reaches an almost constant plateau

value at long times, which indicates the independence of our observations from polymer motion. A representative figure can be found in the Supporting Information (Figure 3s).

It is revealing to combine all droplet data of Figure 2 in a single master plot of Rg_z/Rg_{xy} as a function of the number of chains, n, contained within each droplet. This plot is presented in Figure 3, where it is observed for both adsorption energies that droplets of $n>2$ share a common plateau value of Rg_z/Rg_{xy}, while droplets of $n \leq 2$ gradually attain lower values of Rg_z/Rg_{xy}. The plateau of the n>2 region is also supported by data, which were reported in the literature, as discussed in the introduction.[25, 29, 31-32]

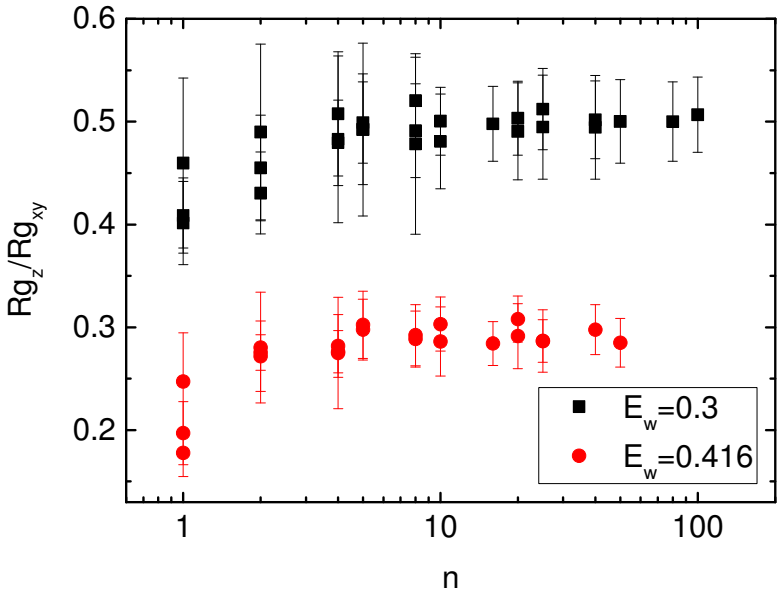

Figure 3: Ratio of the perpendicular to parallel component of the radius of gyration, Rg_z/Rg_{xy}, of the droplets as a function of the number of chains (n) in a droplet, for all the simulated droplets, under weak, $E_w = 0.3$ (black squares), and strong, $E_w = 0.416$ (red circles), adsorption in poor solvent conditions, $E=0.45$.

Further to the discussion above, which was aimed at contrasting single chains with multi-chain droplets, one can separately discuss single chain droplets. It was seen in Figure 2 that

the Rg_z/Rg_{xy} ratio for $N_T=N=1000$ is larger than that for $N_T=N=5000$ and $N_T=N=10000$. One can understand this based on the fact that longer chains tend to adsorb more: the number of adsorbed monomers, and hence the enthalpic gain upon adsorption, increases with increasing N while the entropic cost decreases, as N increases; i.e. the entire chain, due to the many adsorption contacts, may lower its free energy. The preferential adsorption of long chains over shorter chains on a solid surfaces has been reported also by experiments.[59-60] One may, therefore, be witnessing a tendency of the chain to maximize the number of contacts with the substrate with increasing N, subject to the conformational entropic cost per surface-bound monomer. Between $N_T=N=5000$ and $N_T=N=10000$, a difference in Rg_z/Rg_{xy} is noticeable only in the case of stronger adsorption, which is in agreement with this explanation.

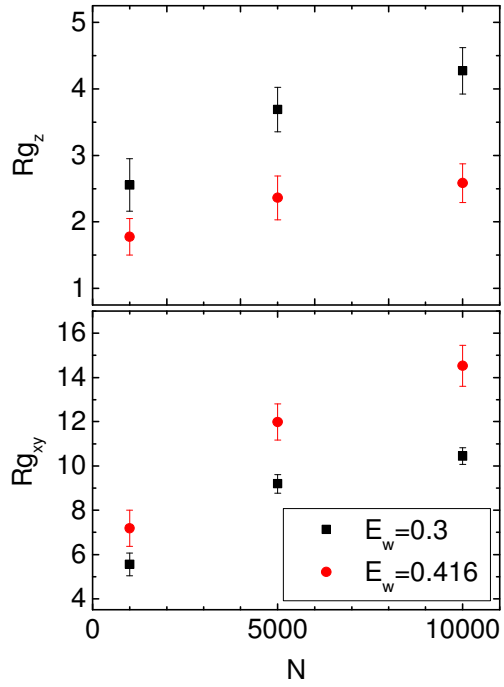

Figure 4: Perpendicular, Rg_z, and horizontal, Rg_{xy}, components of the radius of gyration of single-chain droplets as a function of chain length, N, for $N = N_T = 1000, 5000$, and 10000

under weak, $E_w = 0.3$ (black squares), and strong, $E_w = 0.416$ (red circles), adsorption in poor solvent conditions, $E=0.45$.

Continuing the analysis of single chains, Figure 4 shows the vertical and horizontal components of the radius of gyration, Rg_z and Rg_{xy}, respectively, for the three single chains, $N = 1000, 5000$, and 10000, as functions of N, for both adsorption energies. It is observed that for an overall increase of N by one order of magnitude (from $N = 1000$ to $N = 10000$), Rg_z increases by approximately 1.7 times on the $E_w = 0.3$ substrate and 1.4 times on the $E_w = 0.416$ substrate. Therefore, a rather weak dependence of the perpendicular dimensions of single chains on chain length, N, is observed. This weak dependence is compatible with an increase of Rg_{xy} by approximately 1.9 times for $E_w = 0.3$ and 2.0 times for $E_w = 0.416$, showing that the monomers of each chain are preferentially distributed laterally and this is more pronounced at stronger adsorption conditions. Moreover, the Rg_z dependence on N becomes weaker with increasing N (slope decreases), in agreement with our previous simulation study[13] that the thickness of a single chain adsorbate becomes independent of N as N increases.

Adsorption analysis

In order to gain insight into the wetting behavior of the droplets presented in Figure 2, an analysis is performed of the adsorption behavior of the chains contained within those droplets. Figure 5 shows the dependence of three statistical quantities describing chain adsorption on the length N of the chains that are contained within a droplet: the fraction of adsorbed monomers of a droplet, defined as the number of monomers adjacent to the substrate (one lattice site apart) divided by the total number of monomers contained within a droplet (Figure 5 a, b, c); the fraction of adsorbed chains of a droplet, defined as the number

of chains with at least one adsorbed monomer divided by the total number of chains within a droplet (Figure 5 d, e, f); the average fraction of adsorbed monomers per chain, defined as the number of adsorbed monomers of a chain divided by the total number of monomers of that chain and averaged over all adsorbed chains within a droplet (Figure 5 g, h, i). Figure 5 is divided into three columns, corresponding to the three droplet series for N_T=*1000,* N_T=*5000*, and N_T=*10000*.

The contrast between droplets of single chains and of multi-chain droplets witnessed previously through the Rg_z/Rg_{xy} ratio in Figure 2 is reflected herein, as well, in the difference in the adsorbed monomer fraction between the three single chains, $N_T = N = 1000$, $N_T = N = 5000$, and $N_T = N = 10000$ and the respective multi-chain droplets, in Figures 5a, 5b, and 5c. The higher adsorbed monomer fractions of single chains are in agreement with their lower Rg_z/Rg_{xy} values. As in Figure 2, the single- vs. multi-chain droplet contrast here is more clear in the $N_T = 5000$ and $N_T = 10000$ series and more pronounced for the $E_w = 0.416$ substrate. Comparing droplets across Figures 5 a, 5b, and 5c, it is observed that larger droplets adsorb with a smaller fraction of their monomers and this is true independently of the number of chains contained within the droplets.

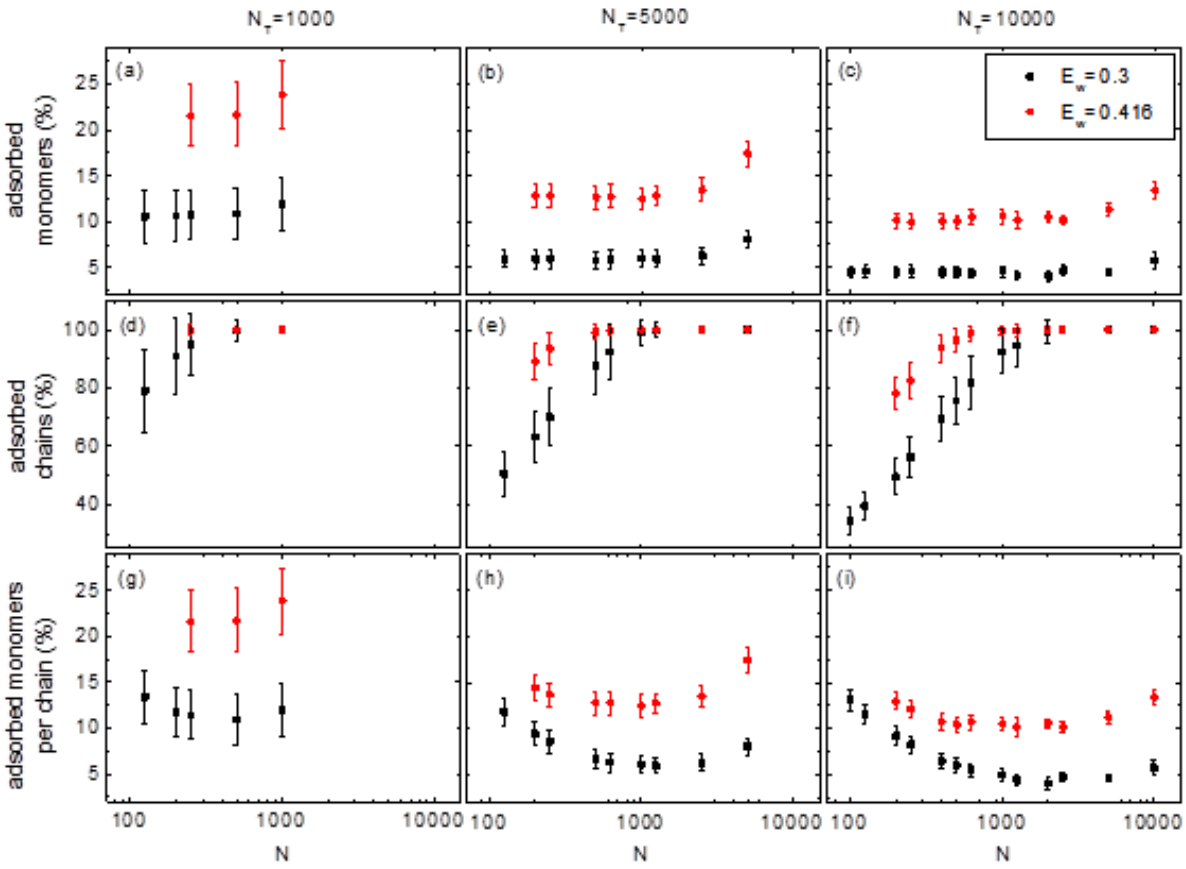

Figure 5: Adsorbed monomers (a, b, c), adsorbed chains (d, e, f), and adsorbed monomers per chain (g, h, i) in percentage form for all simulated droplets, under weak, $E_w = 0.3$ (black squares), and strong, $E_w = 0.416$ (red circles), adsorption under poor solvent conditions, $E=0.45$.

Figures 5d, 5e and 5f illustrate a logarithmic increase of the fraction of adsorbed chains with increasing N or decreasing number of chains, leading to a plateau with all chains making contact with the substrate. The plateau occurs at lower N values for $E_w = 0.416$. Comparing Figures 5d, 5e and 5f one can observe that larger droplets adsorb with a smaller fraction of their chains and reach the maximum adsorption plateau at higher N.

Interesting information about the adsorption process may be extracted by dividing the values of Figures 5a, 5b and 5c by those of Figures 5d, 5e and 5f, respectively, to yield the data in Figures 5g, 5h and 5i, which show the average number of adsorbed monomers per adsorbed chain, in other words, the fraction by which chains adsorb within a droplet on average. In the single chain case ($n = 1$), the flat, pancake-like shape is the result of chain connectivity, whereby adsorbed monomers or trains will drive their neighbors towards the substrate. This type of steric interaction between segments of the same chain or different chains is common in polymer systems.[61] During the transition from a single-chain to a two-chain or a four-chain droplet (going from right to left along the x-axes of the Figures), the fraction of an average chain making contact with the substrate decreases, because the fraction of adsorbed monomers decreases (Figures 5a, 5b and 5c), while the fraction of adsorbed chains remains constant (Figures 5d, 5e and 5f). This implies that monomers belonging to adsorbed segments, i.e., trains, are freed up to become parts of loops. When going from four to more chains in a droplet, a different process dominates. The fraction of an average chain making contact with the substrate increases because the fraction of adsorbed monomers remains constant (Figures 5a, 5b and 5c), while the fraction of adsorbed chains decreases (Figures 5d, 5e and 5f). This implies that chains are freed up as whole entities away from the substrate and move into the bulk of the droplet. Interestingly, this is done in such a way as to maintain a constant number of adsorbed monomers and, hence, constant droplet-substrate adhesive energy. The chains that do remain in contact with the substrate increase their contact by the same number of monomers as that which are freed up as whole chains. Clearly, the minima in Figures 5g, 5h and 5i correspond to the critical thresholds of maximum fraction of adsorbed chains of Figures 5d, 5e and 5f, i.e., they occur at about the same critical N, because they have been calculated by dividing the total number of adsorbed monomers by the fraction of adsorbed chains. For $E_w=0.3$, the critical N-values are about $N=500$, $N=1000$, and $N=2000$

for N_T =*1000,* N_T=*5000*, and N_T=*10000*, respectively, corresponding to a *2*-chain droplet for the N_T=*1000* system and *5*-chain droplets for the two larger systems. For E_w=*0.416*, the critical *N* moves to lower values: about *N=500* and *N=1000* for N_T=*5000* and N_T=*10000*, respectively, which correspond to *10*-chain droplets for the N_T=*5000* and N_T=*10000* systems, whereas it was not accessible for the N_T=*1000* system. This means that the adsorption - desorption threshold occurs at shorter chain length for stronger adsorption. This makes sense if one considers the competition between entropy and enthalpy upon desorption (this will be expanded upon, subsequently). The shorter the chain, the smaller the enthalpic gain and, therefore, the greater the tendency to desorb. A more strongly attractive substrate will work against this tendency.

The above analysis indicates that, for lengths beyond the critical *N*, it is energetically preferable to distribute the droplet-substrate interface unevenly between chains: the fraction of the droplet that makes contact with the surface is maintained by fewer and fewer chains, which become increasingly more strongly adsorbed. In some cases (for N_T = *5000* and N_T = *10000* at E_w = *0.3*), as one goes from the desorption threshold (critical *N*) to the maximum number of chains (minimum *N*), half or more of the chains eventually desorb, while the remaining chains will increase their contact monomers with the substrate by two or more times.

On top of that, this analysis provides insight into the wetting behavior of a droplet via examining the adsorption behavior of its constituent chains. It, therefore, complements the previous wetting analysis in terms of the Rg_z/Rg_{xy} ratio, which treats the droplet as a whole, by providing a detailed account of the behavior of the individual chains and their monomers.

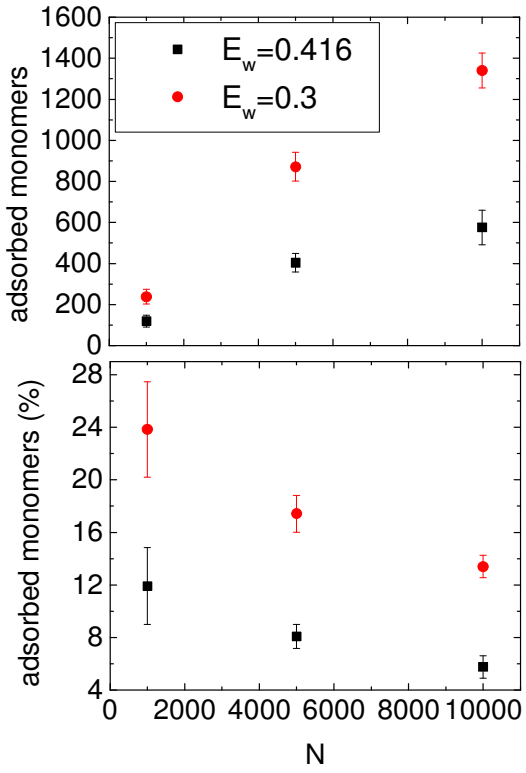

Figure 6: Adsorbed monomers (top) and fraction of adsorbed monomers (bottom) for the three single chains as a function of chain length, N, simulated for weak, $E_w=0.3$ (black squares), and strong, $E_w=0.416$ (red circles), adsorption under poor solvent conditions.

Further to the discussion above, which aimed at describing the transition from single chains to multi-chain droplets, one can separately discuss single chains, as was done in the previous subsection of the wetting analysis. Figure 6 presents the absolute number and the fraction of adsorbed monomers for the three single chains, N = *1000*, *5000*, and *10000* vs their length, N, for both adsorption energies. The number of adsorbed monomers is indicative of how strongly each chain is adsorbed. The absolute number of adsorbed monomers increases monotonically with N, while its percentage relative to the total number of monomers of the

chain monotonically decreases. This phenomenon reflects the tendency of a chain to minimize its potential energy by maximizing the number of contacts with the substrate while reducing its entropic penalty. In simpler terms, longer chains adsorb more strongly. The trend is the same for both substrate potentials. This phenomenon was witnessed from a wetting perspective in the previous subsection as well. At this point it is important to realize that, whereas single chains exhibit a monotonic adsorption trend with *N*, chains in multi-chain droplets do not, as was seen in Figures 5g, 5h and 5i, and the fraction of adsorbed monomers may either increase or decrease, depending on which side of critical *N* they are on.

Shape analysis

Further analysis follows on the shape of single- and multi-chain droplets based on two structural parameters, K_1 and K_2, defined as ratios of the three principal moments $J_{(a)}$ (a = x, y, z) of the gyration tensor (Eqs. (2), (3) and (4)):[62]

$$\boldsymbol{X}_{ab} = \frac{1}{N_T}\sum_{i=1}^{N} \boldsymbol{s}_a^i \boldsymbol{s}_b^i; \quad \boldsymbol{s}^i = \boldsymbol{r}^i - \boldsymbol{r}^{cm} \qquad (2)$$

$$\boldsymbol{X}\cdot\boldsymbol{\omega}^{(a)} = J_{(a)}\boldsymbol{\omega}^{(a)}; \quad a,b = 1,2,3 \qquad (3)$$

$$K_1 = \frac{\langle J_2\rangle + \langle J_3\rangle}{\langle J_1\rangle + \langle J_2\rangle}, \quad K_2 = \frac{\langle J_1\rangle + \langle J_3\rangle}{\langle J_1\rangle + \langle J_2\rangle} \qquad (4)$$

Where N_T is the total number of monomers, $\boldsymbol{r}^{cm}$ is the center of mass of the chain, $\boldsymbol{r}^i$ is the position of the *i-th* segment, and $\boldsymbol{\omega}^{(a)}$, $J_{(a)}$ (a = x, y, z) are the eigenvectors and eigenvalues of $\boldsymbol{X}$. The three eigenvalues are sorted as follows: $J_1 \le J_2 \le J_3$. The quantities K_1 and K_2

assume well known values for typical shapes: For a perfect sphere, $K_1 = K_2 = 1$; for an infinitely thin rod, $K_1 = 0$ and $K_2 = 1$; and for an infinitely thin disk, $K_1 = K_2 = 0.5$.

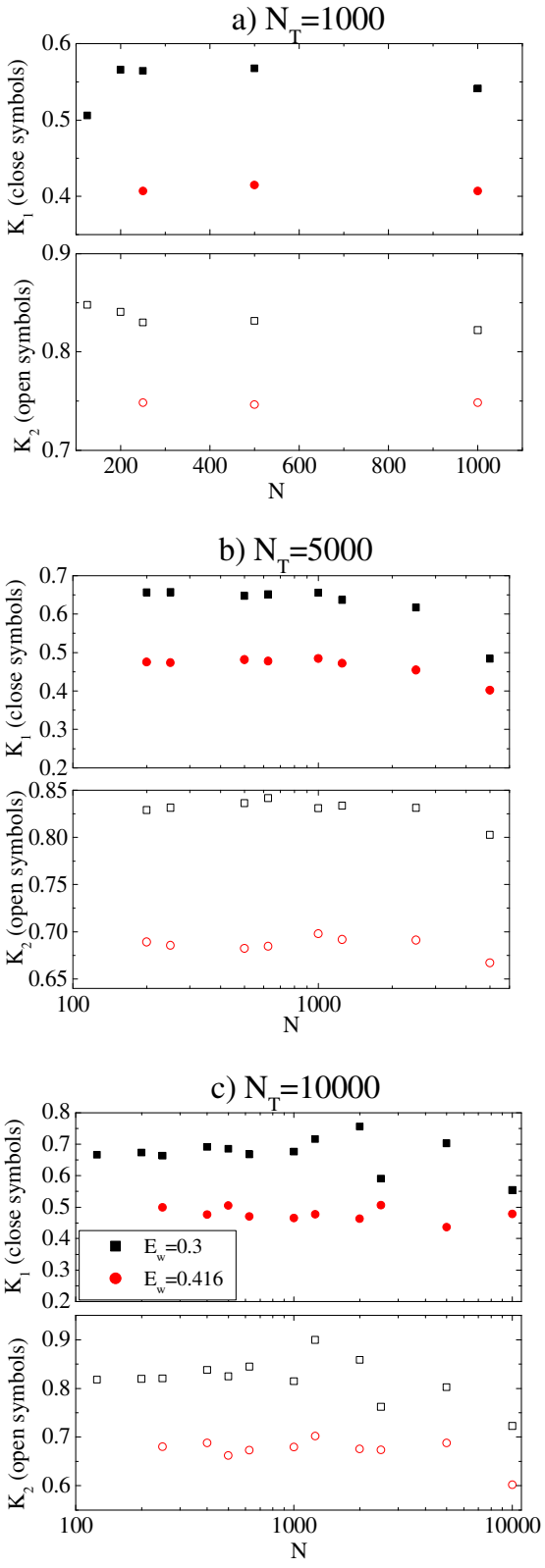

Figure 7*:* Shape parameters K_1 (solid symbols) and K_2 (empty symbols) for (a) N_T=*1000*, (b) N_T=*5000* and (c) N_T=*10000* droplets as a function of chain length, *N*, for all the single- and multi-chain droplets, under weak, E_w = *0.3* (black squares), and strong, E_w = *0.416* (red circles), adsorption under poor solvent conditions, *E=0.45*. Error bars (not visible) are approximately *3%* of the actual values.

K_1 and K_2 values for the series of N_T = *1000*, N_T = *5000*, and N_T = *10000* for both adsorption energies are depicted in Figures 7a, 7b and 7c, respectively, as a function of the length, *N*, of the chains that constitute the droplets. The results indicate the influence of two different factors on the shape of a multi-chain droplet particular size (N_T): the strength of adsorption (i.e., of the surface potential E_w) and the number of chains in the droplets, *n*, as is discussed in the following.

For the smallest droplets, N_T=*1000*, and for both adsorption strengths, K_1 and K_2 indicate a uniaxial prolate ellipsoid for all multi-chain droplets (i.e., for E_w=*0.3*, K_1 ~ *0.55* and K_2 ~ *0.84* and, for E_w=*0.416*, K_1 ~ *0.4* and K_2 ~ *0.75*) somehow more elongated for E_w=*0.3*. For the N_T = *5000* droplets *at* E_w=*0.416*, K_1 ~ *0.47* and K_2 ~ *0.69* and at E_w=*0.3*, K_1 ~ *0.63* and K_2 ~ *0.83*. These values suggest a disk-like "pancake" shape for the case of strong adsorption whereas a prolate ellipsoid is formed at the lower adsorption strength. The N_T = *10000* series follows a similar trend to the N_T = 5000 series for the two adsorption strengths, with slightly higher absolute values of K_1 and K_2. One can therefore see that across all three N_T series (N_T = *1000*, *5000*, *10000*), K_1 and K_2 obtain correspondingly lower values for E_w = *0.416* than E_w = *0.3*. This indicates flatter conformations on strongly adsorbing surfaces and thicker conformations on surfaces of weaker adsorption strength, in line with our previous wetting and adsorption analyses summarized in Figures 2 and 5a-5b-5c), respectively.

Figure 7 also illustrates an effect of the number of chains, n, in a droplet. K_1 and K_2 generally obtain higher values for multi-chain droplets than for single chains. The former share a common plateau, underlying once more the single- vs. multi-chain droplet difference consistently with our previous wetting and adsorption analyses summarized in Figures 2 and 5a-5b-5c, respectively. Also in agreement is the fact that the two larger systems, $N_T = 5000$ and $N_T = 10000$, manifest this difference even more than the smallest one, $N_T = 1000$.

Experimental observations

Figure 8 shows the experimental results from the adsorption of linear polybutadiene, PB, chains on mica: single chains of *962 kg/mol* molecular weight (left column), single chains of *78.8 kg/mol* molecular weight(center column), and multi-chain droplets *78.8 kg/mol* chains (right column). Representative topography tapping-mode AFM images are shown in the top row, while typical AFM-measured profiles are shown in the bottom row. We averaged over several such regions in order to obtain statistically reliable height estimates of the adsorbed PB structures.

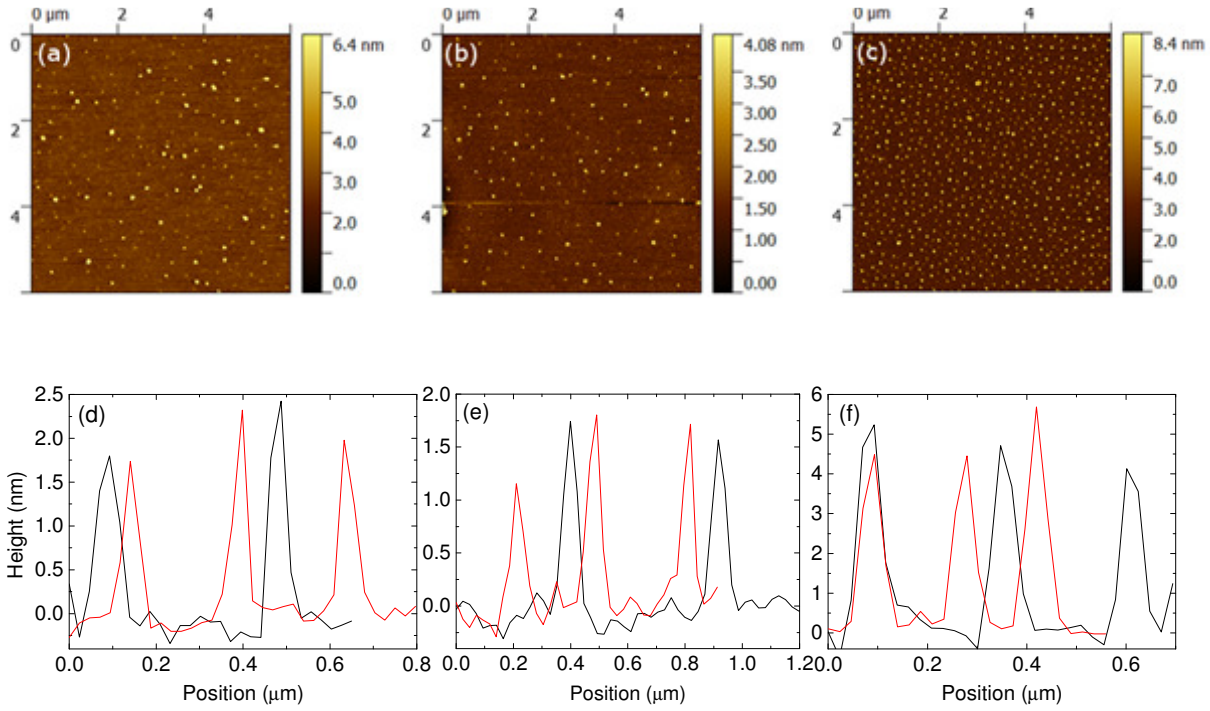

Figure 8: Representative topography tapping-mode AFM images (top) of linear PB on mica and typical AFM-measured profiles (bottom). Left column: single chains with M_w = *962 kg/mol*; center column: single chains with M_w = *78.8 kg/mol*; right column: aggregates of chains with M_w = *78.8 kg/mol*.

Experimental measurements revealed a distinction between multi-chain droplets and single chains of similar size. Specifically, in a measured volume range of 2.5×10^3 *nm*^{3} to 4×10^3 *nm*^{3}, single chains of molecular weight M_w = *962 kg/mol* exhibited adsorbed heights in the range *1.5 nm – 3 nm*, while multi-chain droplets consisting of M_w = *78.8 kg/mol* chains exhibited adsorbed heights in the range *4 nm – 6 nm*. This is in qualitative support of our earlier simulation findings, viz: (a) the smaller Rg_z/Rg_{xy} ratio of single chains relative to chain multi-chain droplets, witnessed in the wetting analysis (Figure 2); (b) the greater percentage of adsorbed monomers of single chains relative to that in multi-chain droplets, witnessed in the adsorption analysis (Figures 5a, 5b, 5c); (c) the lower values of the structural parameters, K_1 and K_2, for single chains relative to multi-chain droplets, witnessed in the shape analysis (Figure 7). Hence, all evidence suggests a fundamental difference in the way in which single chains interact with surfaces compared to (chemically identical) chains in multi-chain droplets.

Experimental measurements also revealed information regarding single-chain adsorption trends. Specifically, adsorbed heights of *1.3 nm* and *2.2 nm* (*±0.5 nm*) were estimated for the *78.8 kg/mol* and *962 kg/mol* single chains, respectively. This experimental result is in qualitative agreement with the simulation result of Figure 4, where it was seen that an overall increase of chain length, *N*, by one order of magnitude (to be compared with a similar fractional increase of molecular weight in the experiment) led to an increase of the vertical component of the radius of gyration, Rg_z, by less than *2* times. The weak dependence of the

perpendicular dimensions of a single chain on chain length, *N*, is, thus, experimentally confirmed.

Conclusions

Different structural compositions of a homopolymer droplet residing on a substrate may have marked effects on the wetting behavior of droplets under poor solvent conditions. One of the most striking results of the present analysis is the differences in the wetting and underlying adsorption mechanism between droplets comprising a single chain and droplets comprised of multi-chains. Whereas single-chain droplets lie flatter and wet the substrate more, chemically identical droplets of ensembles of chains attain a more globular shape and wet the substrate less, as has been witnessed through both computer simulations and experiments. Information on adsorption statistics within droplets, obtained by the computer simulations, shed light on the mechanics of the transition from a single-chain to few-chains to many chains making up droplets of equal total monomer size. A critical conclusion from that information was that isolated chains exhibit a monotonic adsorption trend with chain length, while chains in multi-chain droplets either increase or decrease their adsorbed fraction with chain length depending on their population. This mode of internal chain adsorption allows the droplet as a whole to distribute the droplet-substrate interface in the most energetically preferable way among different chains.

Our coarse grain model offers a qualitative overview of the wetting trends of a polymer droplet. Because the model is minimalistic and relies merely on excluded volume and short-range interactions, it unravels those properties that pertain to the generic adsorbed homopolymer system under poor solvent conditions, irrespectively of chemical specificity.

The simulation results are supported by AFM experiments of linear polybutadiene chains adsorbed on mica.

Having understood the effects of internal arrangement of chains on the wetting and the adsorption behavior, we propose that these can be utilized in the context of a general technique for selecting the appropriate polymer structure for a specific application. This selection should depend on whether more or less wetting is desirable and on how the particular wetting behavior is to be materialized, in terms of internal chain contact with the wetted surface.

Acknowledgements

A.E.A.S.E. acknowledges financial support from the Alexander S. Onassis Public Benefit Foundation, Athens, Greece, for part of this project. A.E.A.S.E. would like to thank Prof. Dimitris Vlassopoulos for illuminating discussions. S.H.A. acknowledges that this research was partially supported by the European Union (European Social Fund, ESF) and Greek national funds through the "ARISTEIA II" Action (SMART_SURF) of the Operational Programme “Education and Lifelong Learning”, NSRF 2007-2013, via the General Secretariat for Research & Technology, Ministry of Education and Religious Affairs, Greece.

ASSOCIATED CONTENT

*S Supporting Information

Additional information concerning the equilibration during the Monte Carlo runs described through the decorrelation of vectors defined on the polymer chain. Conformations of the chain at two different time points during the simulation. Time evolution of the ratio R_{gz}/R_{gxy}.

For Table of Contents Use Only

The Wetting Behavior of Polymer Droplets: Effects of Droplet Size and Chain Length

Apostolos E. A. S. Evangelopoulos, Anastassia N. Rissanou,

Emmanouil Glynos, Ioannis A. Bitsanis,

Spiros H. Anastasiadis and Vasileios Koutsos

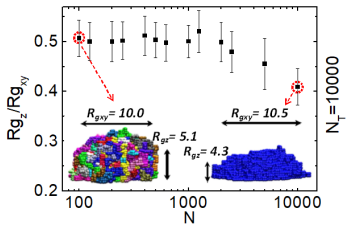

References

1. Goodwin, J., *Colloids and Interfaces with Surfactants and Polymers* 2004.
2. M. Hosseini, A. S. H. M., *Industrial Applications for Intelligent Polymers and Coatings*. 2016.
3. Wei, H.-H.; Li, Y.-C., Conformational transitions of single polymer adsorption in poor solvent: Wetting transition due to molecular confinement induced line tension. *Phys Rev E* **2016,** *94* (1), 012501.
4. D. M. Brewis, D. B., *Industrial Adhesion Problems* 1985.
5. Chremos, A.; Glynos, E.; Koutsos, V.; Camp, P. J., Adsorption and self-assembly of linear polymers on surfaces: a computer simulation study. *Soft Matter* **2009,** *5* (3), 637-645.
6. Chrissopoulou, K.; Andrikopoulos, K. S.; Fotiadou, S.; Bollas, S.; Karageorgaki, C.; Christofilos, D.; Voyiatzis, G. A.; Anastasiadis, S. H., Crystallinity and Chain Conformation in PEO/Layered Silicate Nanocomposites. *Macromolecules* **2011,** *44* (24), 9710-9722.
7. Fotiadou, S.; Chrissopoulou, K.; Frick, B.; Anastasiadis, S. H., Structure and dynamics of polymer chains in hydrophilic nanocomposites. *J Polym Sci Pol Phys* **2010,** *48* (14), 1658-1667.
8. Frank, B.; Gast, A. P.; Russell, T. P.; Brown, H. R.; Hawker, C., Polymer Mobility in Thin Films. *Macromolecules* **1996,** *29* (20), 6531-6534.
9. Glynos, E.; Frieberg, B.; Chremos, A.; Sakellariou, G.; Gidley, D. W.; Green, P. F., Vitrification of Thin Polymer Films: From Linear Chain to Soft Colloid-like Behavior. *Macromolecules* **2015,** *48* (7), 2305-2312.
10. Karaiskos, E.; Bitsanis, I. A.; Anastasiadis, S. H., Monte Carlo studies of tethered chains. *J Polym Sci Pol Phys* **2009,** *47* (24), 2449-2461.
11. Lin, E. K.; Wu, W.-l.; Satija, S. K., Polymer Interdiffusion near an Attractive Solid Substrate. *Macromolecules* **1997,** *30* (23), 7224-7231.
12. Mansfield, K. F.; Theodorou, D. N., Atomistic simulation of a glassy polymer/graphite interface. *Macromolecules* **1991,** *24* (15), 4295-4309.
13. Rissanou, A. N.; Anastasiadis, S. H.; Bitsanis, I. A., A Monte Carlo study of the coil-to-globule transition of model polymer chains near an attractive surface. *J Polym Sci Pol Phys* **2009,** *47* (24), 2462-2476.
14. Rissanou, A. N.; Harmandaris, V., Dynamics of various polymer-graphene interfacial systems through atomistic molecular dynamics simulations. *Soft Matter* **2014,** *10* (16), 2876-2888.
15. Rissanou, A. N.; Harmandaris, V., Structural and Dynamical Properties of Polystyrene Thin Films Supported by Multiple Graphene Layers. *Macromolecules* **2015,** *48* (8), 2761-2772.
16. Vo, L. T.; Anastasiadis, S. H.; Giannelis, E. P., Dielectric study of Poly(styrene-co-butadiene) Composites with Carbon Black, Silica, and Nanoclay. *Macromolecules* **2011,** *44* (15), 6162-6171.
17. Kim, H.; Abdala, A. A.; Macosko, C. W., Graphene/Polymer Nanocomposites. *Macromolecules* **2010,** *43* (16), 6515-6530.
18. RamanathanT; Abdala, A. A.; StankovichS; Dikin, D. A.; Herrera Alonso, M.; Piner, R. D.; Adamson, D. H.; Schniepp, H. C.; ChenX; Ruoff, R. S.; Nguyen, S. T.; Aksay, I. A.; Prud'Homme, R. K.; Brinson, L. C., Functionalized graphene sheets for polymer nanocomposites. *Nat Nano* **2008,** *3* (6), 327-331.
19. Tran, M. Q.; Cabral, J. T.; Shaffer, M. S. P.; Bismarck, A., Direct measurement of the wetting behavior of individual carbon nanotubes by polymer melts: The key to carbon nanotube-polymer composites. *NANO LETTERS* **2008,** *8*, 2744-2750.
20. Rissanou, A.; Power, A.; Harmandaris, V., Structural and Dynamical Properties of Polyethylene/Graphene Nanocomposites through Molecular Dynamics Simulations. *Polymers* **2015,** *7* (3), 390.

21. Boyce, J. F.; Hovanes, B. A.; Harris, J. M.; Van Alstine, J. M.; Brooks, D. E., The wetting behavior of aqueous two-phase polymer test systems on dextran coated glass surfaces: Effect of molecular weight. *J Colloid Interf Sci* **1992,** *149* (1), 153-161.
22. Dee, G. T.; Sauer, B. B., The molecular weight and temperature dependence of polymer surface tension: Comparison of experiment with interface gradient theory. *J Colloid Interf Sci* **1992,** *152* (1), 85-103.
23. Jalbert, C.; Koberstein, J. T.; Hariharan, A.; Kumar, S. K., End Group Effects on Surface Properties of Polymers: Semiempirical Calculations and Comparison to Experimental Surface Tensions for α,ω-Functional Poly(dimethylsiloxanes). *Macromolecules* **1997,** *30* (15), 4481-4490.
24. Jalbert, C.; Koberstein, J. T.; Yilgor, I.; Gallagher, P.; Krukonis, V., Molecular weight dependence and end-group effects on the surface tension of poly(dimethylsiloxane). *Macromolecules* **1993,** *26* (12), 3069-3074.
25. Willson, K. R.; Garoff, S., Effect of chain termination chemistry and molecular weight on dynamic wetting of polymer liquids. *Colloids and Surfaces A: Physicochemical and Engineering Aspects* **1994,** *89* (2), 263-268.
26. Qian, Z.; Minnikanti, V. S.; Sauer, B. B.; Dee, G. T.; Archer, L. A., Surface Tension of Symmetric Star Polymer Melts. *Macromolecules* **2008,** *41* (13), 5007-5013.
27. Glynos, E.; Chremos, A.; Frieberg, B.; Sakellariou, G.; Green, P. F., Wetting of Macromolecules: From Linear Chain to Soft Colloid-Like Behavior. *Macromolecules* **2014,** *47* (3), 1137-1143.
28. Glynos, E.; Frieberg, B.; Green, P. F., Wetting of a Multiarm Star-Shaped Molecule. *Phys Rev Lett* **2011,** *107* (11), 118303.
29. Milchev, A.; Binder, K., Polymer melt droplets adsorbed on a solid wall: A Monte Carlo simulation. *J Chem Phys* **2001,** *114* (19), 8610-8618.
30. Milchev, A.; Milchev, A.; Binder, K., Nanodroplets on a solid plane: wetting and spreading in a Monte Carlo simulation. *Computer Physics Communications* **2002,** *146* (1), 38-53.
31. Heine, D. R.; Grest, G. S.; Webb, E. B., Spreading dynamics of polymer nanodroplets. *Phys Rev E* **2003,** *68* (6), 061603.
32. Dhondi, S.; Pereira, G. G.; Hendy, S. C., Effect of Molecular Weight on the Capillary Absorption of Polymer Droplets. *Langmuir* **2012,** *28* (27), 10256-10265.
33. Pattanayek, S. K.; Pereira, G. G., Shape of Micelles Formed From Strongly Adsorbed Grafted Polymers in Poor Solvents. *Macromol Theor Simul* **2005,** *14* (6), 347-357.
34. Tagliazucchi, M.; Szleifer, I., Stimuli-responsive polymers grafted to nanopores and other nano-curved surfaces: structure, chemical equilibrium and transport. *Soft Matter* **2012,** *8* (28), 7292-7305.
35. Pattanayek, S. K.; Pham, T. T.; Pereira, G. G., Morphological structures formed by grafted polymers in poor solvents. *J Chem Phys* **2005,** *122* (21), 214908.
36. Jentzsch, C.; Sommer, J. U., Polymer brushes in explicit poor solvents studied using a new variant of the bond fluctuation model. *J Chem Phys* **2014,** *141* (10), 104908.
37. Peleg, O.; Tagliazucchi, M.; Kröger, M.; Rabin, Y.; Szleifer, I., Morphology Control of Hairy Nanopores. *ACS Nano* **2011,** *5* (6), 4737-4747.
38. Bitsanis, I. A.; Brinke, G. t., A lattice Monte Carlo study of long chain conformations at solid–polymer melt interfaces. *J Chem Phys* **1993,** *99* (4), 3100-3111.
39. Marcus, M.; Luis González, M., Wetting of polymer liquids: Monte Carlo simulations and self-consistent field calculations. *J Phys-Condens Mat* **2003,** *15* (19), R609.
40. Schmid, F., Self-consistent-field theories for complex fluids. *J Phys-Condens Mat* **1998,** *10* (37), 8105.
41. Smith, G. D.; Yoon, D. Y.; Jaffe, R. L., Conformations of polymer melts between parallel surfaces: comparison of the Scheutjens-Fleer lattice theory with Monte Carlo simulations. *Macromolecules* **1992,** *25* (25), 7011-7017.

42. Yethiraj, A., In *Polymer Melts at Solid Surfaces, Advances in Chemical Physics*, Ed. I. Prigogine, S. A. R. J. W. S., Inc., 2002, Ed. 2002; Vol. 121.
43. Eisenriegler, E., *Polymers at Surfaces* 1993.
44. Gennes, P.-G. d., *Scaling Concepts in Polymer Physics* 1979.
45. Granick, S., In *Polymers in Confined Environments, Advances in Polymer Science* Springer, Ed. Berlin, 1999; Vol. 138.
46. K. Binder, e., *The Monte Carlo Method in Condensed Matter Physics* 1995.
47. De Gennes, P. G., Scaling theory of polymer adsorption. *J. Phys. France* **1976,** *37* (12), 1445-1452.
48. M. Rubinstein, R. H. C., *Polymer Physics* 2003.
49. Möddel, M.; Bachmann, M.; Janke, W., Conformational Mechanics of Polymer Adsorption Transitions at Attractive Substrates. *J Phys Chem B* **2009,** *113* (11), 3314-3323.
50. Evangelopoulos, A. E. A. S.; Glynos, E.; Madani-Grasset, F.; Koutsos, V., Elastic Modulus of a Polymer Nanodroplet: Theory and Experiment. *Langmuir* **2012,** *28* (10), 4754-4767.
51. Rissanou, A. N.; Anastasiadis, S. H.; Bitsanis, I. A., Monte Carlo study of the coil-to-globule transition of a model polymeric system. *J Polym Sci Pol Phys* **2006,** *44* (24), 3651-3666.
52. Lax, M.; Brender, C., Monte Carlo study of lattice polymer dynamics. *J Chem Phys* **1977,** *67* (4), 1785-1787.
53. Mandel, F., Macromolecular dimensions obtained by an efficient Monte Carlo method: The mean square end-to-end separation. *J Chem Phys* **1979,** *70* (8), 3984-3988.
54. Miros, A.; Vlassopoulos, D.; Likhtman, A. E.; Roovers, J., Linear rheology of multiarm star polymers diluted with short linear chains. *J. Rheol.* **2003,** *47* (1), 163-176.
55. Markiewicz, P.; Goh, M. C., Atomic force microscopy probe tip visualization and improvement of images using a simple deconvolution procedure. *Langmuir* **1994,** *10* (1), 5-7.
56. Glynos, E.; Chremos, A.; Petekidis, G.; Camp, P. J.; Koutsos, V., Polymer-like to Soft Colloid-like Behavior of Regular Star Polymers Adsorbed on Surfaces. *Macromolecules* **2007,** *40* (19), 6947-6958.
57. Roovers, J., Concentration Dependence of the Relative Viscosity of Star Polymers. *Macromolecules* **1994,** *27* (19), 5359-5364.
58. McClements, J.; Buffone, C.; Shaver, M. P.; Sefiane, K.; Koutsos, V., Poly(styrene-co-butadiene) random copolymer thin films and nanostructures on a mica surface: morphology and contact angles of nanodroplets. *Soft Matter* **2017,** *13* (36), 6152-6166.
59. Kawaguchi, M.; Hattori, S.; Takahashi, A., Ellipsometric study of competitive and displacement adsorption of polymers at the .THETA. condition. *Macromolecules* **1987,** *20* (1), 178-180.
60. Kawaguchi, M.; Maeda, K.; Kato, T.; Takahashi, A., Preferential adsorption of monodisperse polystyrene on silica surface. *Macromolecules* **1984,** *17* (9), 1666-1671.
61. JOHNSON, H. E.; GRANICK, S., New Mechanism of Nonequilibrium Polymer Adsorption. *Science* **1992,** *255* (5047), 966-968.
62. Ivanov, V. A.; Stukan, M. R.; Vasilevskaya, V. V.; Paul, W.; Binder, K., Structures of stiff macromolecules of finite chain length near the coil-globule transition: A Monte Carlo simulation. *Macromol Theor Simul* **2000,** *9* (8), 488-499.